energies

MDPI

Article

Thermal Model Approach to the YASA Machine for In-Wheel Traction Applications

Guangchen Wang [1], Yingjie Wang [2], Yuan Gao [3], Wei Hua [4], Qinan Ni [5] and Hengliang Zhang [4,*]

[1] Taizhou Liangsu Technology Co., Ltd., Taizhou 318016, China; m15909828335@163.com
[2] Tangshan Power Supply Company, State Grid Jibei Power Co., Ltd., Tangshan 063000, China; yjwang1995@163.com
[3] Department of Aerospace Engineering, Faculty of Engineering, University of Bristol, Queens Road, Bristol BS8 1QU, UK; yuan21.gao@bristol.ac.uk
[4] School of Electrical Engineering, Southeast University, Nanjing 210096, China; huawei1978@seu.edu.cn
[5] Jiangsu Yueda Group, Yancheng 224007, China; niqn_hit@163.com
* Correspondence: zhanghengliang@seu.edu.cn

Abstract: The axial-flux permanent magnet (AFPM) machines with yokeless and segmented armature (YASA) topology are suitable for in-wheel traction systems due to the high power density and efficiency. To guarantee the reliable operation of the YASA machines, an accurate thermal analysis should be undertaken in detail during the electrical machine design phase. The technical contribution of this paper is to establish a detailed thermal analysis model of the YASA machine by the lumped parameter thermal network (LPTN) method. Compared with the computational fluid dynamics (CFD) method and the finite element (FE) method, the LPTN method can obtain an accurate temperature distribution with low time consumption. Firstly, the LPTN model of each component of the YASA machine is constructed with technical details. Secondly, the losses of the YASA machine are obtained by the electromagnetic FE analysis. Then, the temperature distribution of the machine can be calculated by the LPTN model and loss information. Finally, a prototype of the YASA machine is manufactured and its temperature distribution under different operating conditions is tested by TT-K-30 thermocouple temperature sensors. The experimental data matches the LPTN results well.

Keywords: lumped parameter thermal network (LPTN); losses; temperature distribution; yokeless and segmented armature (YASA)

Citation: Wang, G.; Wang, Y.; Gao, Y.; Hua, W.; Ni, Q.; Zhang, H. Thermal Model Approach to the YASA Machine for In-Wheel Traction Applications. *Energies* **2022**, *15*, 5431. https://doi.org/10.3390/en15155431

Academic Editor: Federico Barrero

Received: 7 July 2022
Accepted: 25 July 2022
Published: 27 July 2022

1. Introduction

Electric vehicles driven by four in-wheel electrical machines make the traction system more simplified and flexible [1]. In the limited volume, the yokeless and segmented armature (YASA) axial flux machine is capable of producing larger torque compared with radial flux machines [2–5]. The yokeless segmented stator core and the centralized short-distance windings make it more efficient and give it a higher power density [6,7]. Therefore, YASA machines are potential candidates for in-wheel traction applications.

It is well-known that losses cause the temperature rise of electrical machines, which can weaken the machine's performance and even damage electrical machines [8]. The insulation system of armature winding and thermal characteristics of the permanent magnet limits the maximum temperature of the electrical machines. The YASA machines feature a high power density, which means a high loss density as well [9,10]. When machines produce the peak torque under the peak current, a high copper loss is generated, making the winding temperature rise rapidly. That challenges the insulation system of the electrical machine. To ensure the reliability of the YASA machine, the thermal performance should be thoroughly considered [11,12].

There are three typical methods for the thermal analysis of YASA machines, i.e., the computational fluid dynamics (CFD) method, the finite element (FE) method, and

the lumped parameter thermal network (LPTN) method [13–21]. The CFD method can calculate the convective heat transfer coefficients, which are significant in electrical machine design [1,13]. However, the CFD model is usually complicated, which means it requires several days or even a week to establish and calculate the thermal model [14]. In [15], a novel stator cooling structure is introduced to improve the temperature distribution of the YASA machine, and the CFD method verifies the proposed cooling structure. The CFD method is applied in [16] to calculate an innovative water-cooling system for the YASA machine. The FE method can obtain an accurate temperature distribution, but it requires several hours to calculate the model and the boundary processing is complicated and difficult [17,18]. In [17], both analytical and experimental investigations into the air-cooling of a YASA motor for in-wheel traction are presented. In [18], a stator heat extraction system for YASA machines is introduced and modeled, and the thermal analysis is calculated by the FE method. The LPTN method divides the electrical machine into several nodes corresponding to the machine components and the heat-source distribution [19,20], which can guarantee the analysis accuracy while keeping it fast compared with the CFD and FE methods. For machines with complex structures, accurate temperature distribution can be quickly obtained by LPTN. Therefore, this paper only focuses on a LPTN model of the YASA machine.

To the best of our knowledge, only a few papers have used the LPTN method to compute the temperature distribution of YASA machines. For example, in [21], the short-time duty and the intermittent duty of a 4 kW YASA machine are calculated based on the LPTN method. In [22], a lumped parameter T-type thermal network model is applied to the YASA machine temperature calculation, but it mainly focuses on the calculation of core loss rather than the total losses. In [23], a 3D LPTN model is developed and experimentally validated, where the air-cooling channels between permanent magnets on the rotor plates are also considered. However, it only constructs the thermal models of the stator (including the armature winding and stator core) and rotor without considering the other components of the YASA machine. The main technical contribution of this paper is to use the LPTN method to construct a detailed thermal model for the YASA machine including all components. The temperature distribution of the YASA machine is obtained rapidly and accurately by considering the losses calculated by the FE method. The LPTN model can provide a reference for the thermal analysis of YASA machines, which not only ensures the thermal reliability of the machine, but also saves time and calculation resources in the machine design phase.

This report is arranged as follows: In Section 2, the topology of the YASA machine is introduced, and the corresponding design parameters are listed. Then, in Section 3, the detailed thermal model of the YASA machine is established, and the corresponding thermal resistance of all components is deduced. To obtain the temperature distribution, the calculated losses are introduced into the entire thermal model of the YASA machine, as described in Section 4. After that, in Section 5, the prototype test proves the accuracy of the thermal network model. Finally, this paper is concluded in Section 6.

2. Topology of the Studied YASA Machine

In this section, the structure and design parameters of the YASA machine are introduced.

2.1. Structure

Similar to the radial-flux permanent magnet (RFPM) machines, the YASA machines belong to the category of permanent magnet (PM) machines. However, the magnetic flux in the air gap of YASA machines is different from that of the RFPM machines. The magnetic flux of the YASA machines is along the axial direction in the air gap, while that of the RFPM machines is along the radial direction. Compared with the conventional RFPM machines, the YASA machines can generate a higher performance when the radial diameter is larger than the axial length [1,8,17].

The YASA machines consist of a yokeless and segmented stator and double external rotors [8]. The main magnetic flux of YASA machines, shown in Figure 1, starts from the N-pole permanent magnet and passes through the stator core to the S-pole on the other side. After passing through the rotor core on the second side, the flux starts from the N-pole on the second side and passes through the stator core to the S-pole of the first side. Finally, the main magnetic flux forms a closed loop.

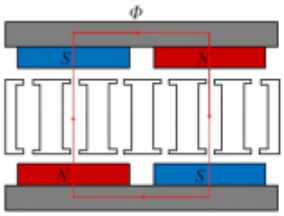

Figure 1. The main magnetic flux of the YASA machines.

The construction of YASA machines possesses many significant advantages. The segmented stator core equipped with a concentrated winding having short end-windings that result in a high filling factor and low copper losses. The structure of a yokeless stator is beneficial to decreasing mass and core loss [1,8,17]. In addition, YASA machines generally exhibit low self-inductance and mutual inductances among the phases, which improve fault tolerance and operation reliability [16,19].

The YASA machine investigated in this paper is shown in Figure 2, where the *x*-axis, *y*-axis, and *z*-axis, respectively, represent the circumferential direction, axial direction, and radical direction. The YASA machine can be divided into the stationary part and rotating part, where the stationary part includes the stator core, armature winding, supporting frame, and shaft, and the rotating part includes permanent magnets, rotor core, and the housing.

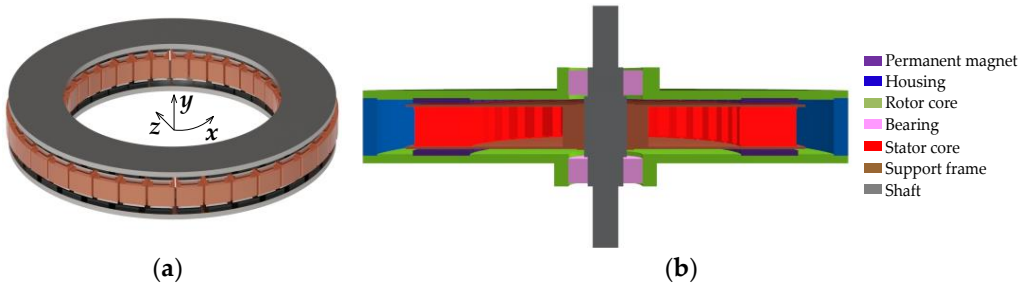

Figure 2. Structure of the YASA machine: (**a**) 3-dimensional structure; (**b**) view of the cross-section.

2.2. Design Parameters

A 5 kW prototyped machine was developed to validate the thermal analysis of the YASA machine. The main performance and geometric parameters are listed in Table 1.

Table 1. Key parameters of the studied YASA machine.

Parameters	Values	Parameters	Values
DC voltage (V)	72	Active outer diameter (mm)	270
Rated power (kW)	5	Active internal diameter (mm)	190
Rated speed (r/min)	480	Active axial length (mm)	45
Rated torque (Nm)	99	Rotor core thickness (mm)	4.8
Rated current (Arms)	17	Permanent magnet thickness (mm)	3.4
Slot number	36	Pole arc coefficient	0.83
Pole number	32	Air gap (mm)	0.9

3. Construction of the LPTN Model

In this section, the LPTN models of different components of the YASA machine are constructed. Generally, there are three main parts taken into account, i.e., the stationary part, the rotating part, and the YASA machine assembly. The thermal model of the YASA machine involves many parameters (including geometric parameters and heat transfer coefficients). The geometric parameters of the YASA machine are determined by the intelligent optimization algorithm in the machine design process. Additionally, the heat transfer coefficients are identified by fine-tuning against simple test data through a genetic algorithm [24].

3.1. Thermal Model of the Stationary Part

In this subsection, the thermal model of the stationary part is introduced, which includes the armature winding, stator core, support frame, and shaft.

3.1.1. Armature Winding

The armature winding is the main heat source, especially when operating at peak torque with peak current. The heat dissipation of the armature winding is difficult, because the winding is in the middle of the YASA machine. Additionally, the winding is relatively dispersed, resulting in uneven temperature distribution. Hence, it is difficult to build a detailed thermal model.

This paper uses the layered winding model from [25], in which the coil of the armature winding is regarded as a uniform heat conduction material. The actual thermal conductivity is replaced by an equivalent thermal conductivity k_{wd}.

The armature winding includes the outer end-winding, inner end-winding, and slot-winding. Figure 3 shows the specific position of the armature winding. Each section of the armature winding is represented in Figure 4. The numbers in Figure 4 correspond to those marked in Figure 3.

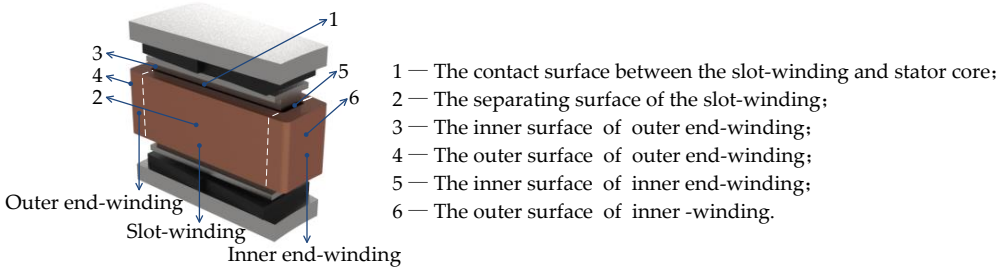

Figure 3. Position in the cross-section of the segmented stator.

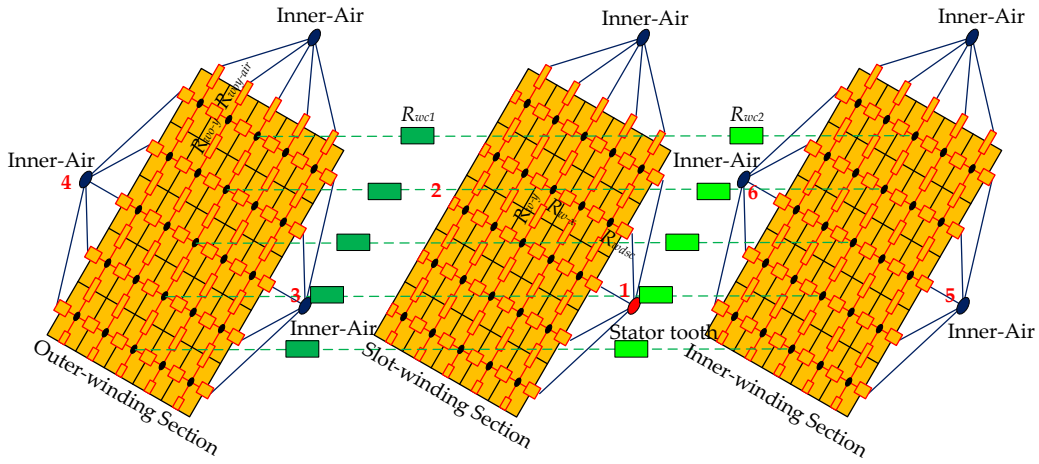

Figure 4. The thermal model of a single segmented armature winding.

For both the inner and outer end-winding, axial thermal resistances (R_{wo-y}, $R_{woy-air}$, R_{wo-ya}, R_{w-y}) and radial thermal resistance (R_{w-x}) are considered. Since the axial cross-section of the end-windings remains unchanged, the axial thermal resistances are approximately constant. The radial thermal resistance changes with the radius. For instance, the axial thermal resistance of the outer end-winding is

$$R_{wo-y} = \frac{L_{wo-y}}{k_{wd} S_{wo-y}} \tag{1}$$

where L_{wo-y} is the distance of adjacent nodes at the outer end-winding, and S_{wo-y} is the area of the corresponding region between nodes, as shown in Figure 4.

Between the outer end-winding and inner-air (including the air gap and air inside the YASA machine), there are axial thermal resistances $R_{woy-air}$ and R_{wo-ya}.

$$R_{woy-air} = \frac{1}{2} R_{wo-y} + R_{wo-ya} \tag{2}$$

$$R_{wo-ya} = \frac{1}{k_{wdout} S_{wo-y}} \tag{3}$$

where R_{wo-ya} is the convective thermal resistance and k_{wdout} is the equivalent convective heat transfer coefficient.

Similarly, the cross-section of slot-winding is constant. The thermal resistances of the slot-winding (including the axial thermal resistance R_{w-y} and radial thermal resistance R_{w-x}) are regarded as unchanged. The expressions follow:

$$R_{w-y} = \frac{\frac{H_{wd}}{2}/5}{\left(\frac{W_{wd}}{2}/5 \times L_s\right) \times k_{wd}} \tag{4}$$

$$R_{w-x} = \frac{\frac{W_{wd}}{2}/5}{\left(\frac{H_{wd}}{2}/5 \times L_s\right) \times k_{wd}} \tag{5}$$

where W_{wd} and H_{wd} represent the width and height of slot-winding, respectively. L_s is the difference between the outer and inner radius of the stator core.

When calculating the thermal resistance R_{wdsc} between the slot-winding and stator core, the thermal resistance of slot insulation should be taken into account:

$$R_{wdsc} = \frac{1}{2} R_{w-x} + R_{lx-s} + R_{scx} \tag{6}$$

$$R_{lx-s} = \frac{W_l}{\left(\frac{H_{wd}}{2}/5 \times L_s\right) \times k_l} \tag{7}$$

where R_{lx-s} is the thermal resistance of the slot insulation, W_l is the equivalent thickness of the slot insulation, k_l is the equivalent thermal conductivity of the slot insulation, and Rs_{cx} is the thermal resistance of the stator core along the x-axis. In addition, there are thermal resistances R_{wc1} and R_{wc2} between the slot-winding and both end-windings, respectively, as shown in Figure 4.

3.1.2. Stator Core

The complete thermal model of the stator is shown in Figure 5. It should be noted that the thermal model of the armature winding and segmented stator core can be consolidated into a single node [19]. R_{ciax} and R_{ciay} are the equivalent thermal resistance of the armature winding along the x-axis and y-axis, respectively. R_{lx} is the thermal resistance of the slot insulation. R_{wia} is the convective thermal resistance between the armature winding and inner-air. $P_{w,slot}$ and $C_{w,slot}$ represent the loss and heat capacity of the 1/4 slots, respectively.

$P_{sc,slot}$ and $C_{sc,slot}$ represent the loss and heat capacity of the 1/2 stator core, respectively. The heat capacity is defined as follows:

$$C_x = c_x m_x \tag{8}$$

where m_x and c_x are the mass and heat capacity, respectively.

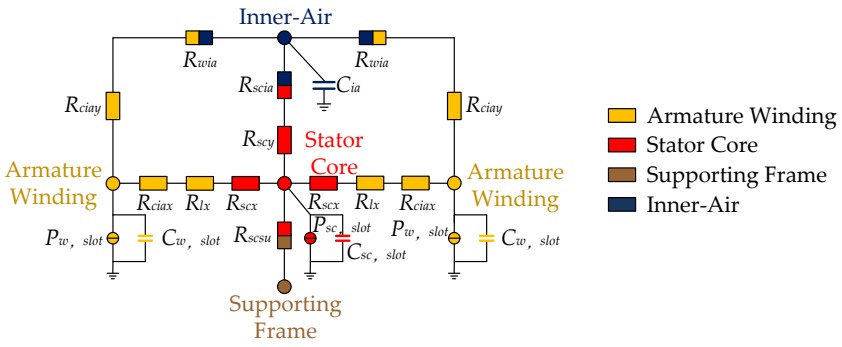

Figure 5. Thermal model of the single-segmented stator.

R_{scx} and R_{scy} are the thermal resistances of the stator core along the x-axis and y-axis, respectively. The calculations are as follows:

$$R_{scx} = \frac{W_{st}/2}{\frac{H_{st}}{2} \times L_s k_{iron}} \tag{9}$$

$$R_{scy} = \frac{H_{st}/4}{W_{st} L_s k_{iron}} \tag{10}$$

where W_{st} and H_{st} are the width and height of the stator core, respectively, and k_{iron} is the thermal conductivity of the stator core.

Owing to the symmetrical structure, Figure 5 can be further simplified to Figure 6. Figure 6 is the thermal model of the stator core, which constitutes the entire thermal model of the YASA machine (discussed in Section 3.3). P_w and C_w represent half of the copper loss and heat capacity. P_{sc} and C_{sc} represent half of the stator core loss and heat capacity. The convective thermal resistance between the stator core and inner-air present is R_{scia}.

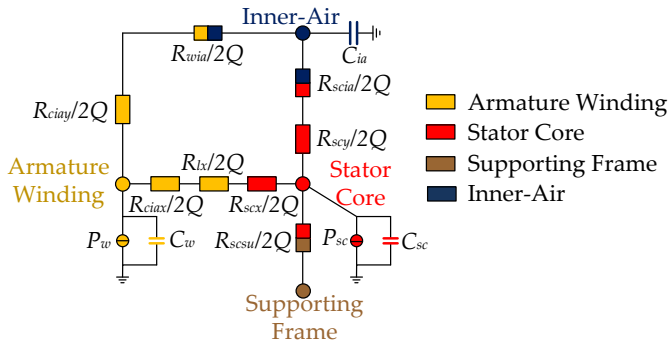

Figure 6. Simplified thermal model of the segmented stator.

3.1.3. Support Frame

The segmented stator core is shown in Figure 7a. In Figure 7b, there are matched cages on both sides of the segmented stator cores for support. The cages are connected by a circular connector with a support frame.

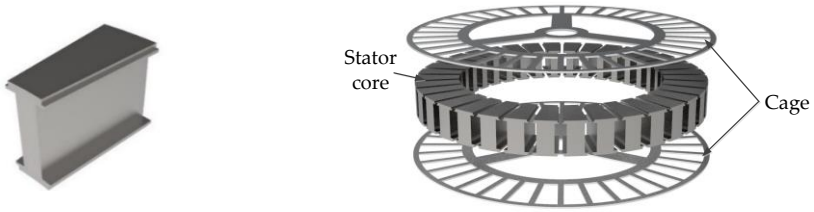

Figure 7. Stator: (**a**) segmented stator core; (**b**) stator core and cages.

The thermal model of the support frame is shown in Figure 8. The support frame connects with the stator core and shaft. The thermal resistance between the support frame and stator core is R_{scsu}, as shown in Figure 6. The thermal resistance between the support frame and shaft is R_{sush}. In addition, there is thermal resistance R_{suia} between the support frame and inner-air. The calculation equations follow:

$$R_{scsu} = \frac{l_{scsu}}{S_{scsu} k_{air}} \tag{11}$$

$$R_{sush} = \frac{l_{sush}}{S_{sush} k_{air}} \tag{12}$$

$$S_{sush} = 2\pi R_{sui} \frac{H_{su}}{2} = \pi R_{sui} H_{su} \tag{13}$$

where l_{scsu} is the tolerance clearance between the support frame and stator core, l_{sush} is the tolerance clearance between the support frame and shaft, S_{scsu} is the area of the tolerance clearance between the support frame and stator core, S_{sush} is the area of the tolerance clearance between the support frame and shaft, and k_{air} is the thermal conductivity of air. R_{sui} and H_{su} are the inner radius and height of the connector.

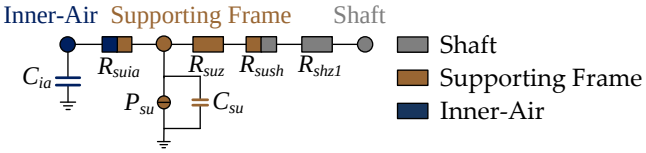

Figure 8. The thermal model of the support frame.

3.1.4. Shaft

Figure 9 shows the thermal model of shaft, where R_{shz1} represents the radial thermal resistance from the support frame to shaft, R_{shz2} is the radial thermal resistance from the shaft to bearing, R_{shy1} is the axial thermal resistance between the shaft and bearing, R_{shy2} is the axial thermal resistance from the bearing to shaft end, R_{shso} is convective thermal resistance between the shaft and surroundings. Additionally, there is convection thermal resistance R_{shia} between the shaft and inner-air. The thermal resistances are calculated as follows:

$$R_{shz1} = \frac{d_{sh1}/2}{(\pi d_{sh1}/2)\frac{H_{sh}}{2} k_{sh}} = \frac{2}{\pi H_{sh} k_{sh}} \tag{14}$$

$$R_{shz2} = \frac{d_{sh2}/2}{(\pi d_{sh2}/2) H_{be} k_{sh}} = \frac{1}{\pi H_{be} k_{sh}} \tag{15}$$

$$R_{shy1} = \frac{l_{sh1}/4}{\pi (d_{sh1}/2)^2 k_{sh}} + \frac{l_{sh2}/2}{\pi (d_{sh2}/2)^2 k_{sh}} \tag{16}$$

$$R_{shy2} = \frac{l_{sh2}/2}{\pi (d_{sh2}/2)^2 k_{sh}} + \frac{l_{sh3}/2}{\pi (d_{sh3}/2)^2 k_{sh}} \tag{17}$$

$$R_{shso} = \frac{1}{S_{shso} k_{shso}} \tag{18}$$

$$S_{shso} = \pi (d_{sh3}/2)^2 + \pi d_{sh3} l_{sh3} \tag{19}$$

where k_{sh} is the thermal conductivity of the shaft, k_{shso} is the convective heat transfer coefficient between the shaft and surroundings, and H_{be} is the height of the bearing. The other structural parameters are defined in Figure 10.

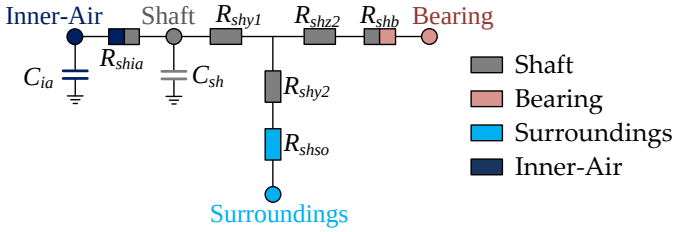

Figure 9. Thermal model of the shaft.

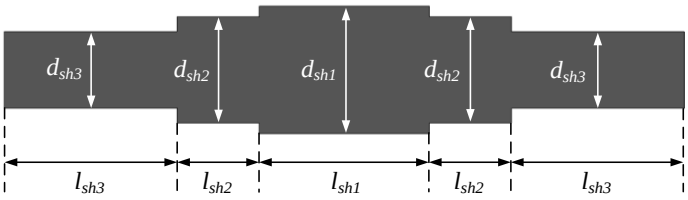

Figure 10. Structure of the shaft.

3.2. Thermal Model of the Rotating Part

In this subsection, the thermal model of the rotating part is introduced, which includes the permanent magnets, bearing, rotor core, and housing.

3.2.1. Permanent Magnet

Figure 11 shows the thermal model of the permanent magnet, where R_{mia} is the convective thermal resistance between the permanent magnet and inner-air, R_{my} is the axial thermal resistance of the permanent magnet, R_{mrc} is the thermal resistance between the permanent magnet and rotor core, and R_{rcy} is the axial thermal resistance of rotor core.

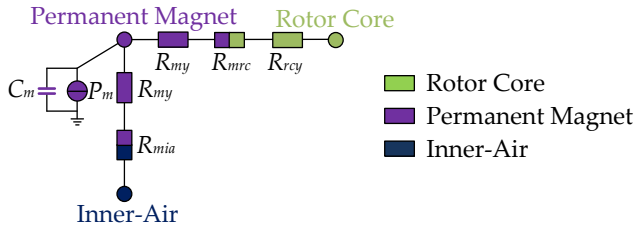

Figure 11. Thermal model of the permanent magnet.

The equations of R_{my}, R_{mcr} and R_{rcy} follow:

$$R_{my} = \frac{H_m/2}{S_m k_m} \tag{20}$$

$$R_{mrc} = \frac{l_{mr}}{S_m k_{air}} \tag{21}$$

$$R_{rcy} = \frac{H_{rc}/2}{S_{rc} k_{rc}} \tag{22}$$

$$S_{rc} = \pi\left(r_{rco}^2 - r_{rci}^2\right) \tag{23}$$

where H_m and H_{rc} are the thicknesses of the permanent magnet and rotor core, respectively. S_m, S_{rc} is the radial cross-section area of the permanent magnet and rotor core, respectively; k_m, k_{rc} is the thermal conductivity of permanent magnet and rotor core, respectively. The tolerance clearance between the permanent magnet and rotor core is l_{mr}; r_{rco}, r_{rci} is the outer and inner radius of the rotor core, respectively. The components of the machine cross-section are illustrated in Figure 12.

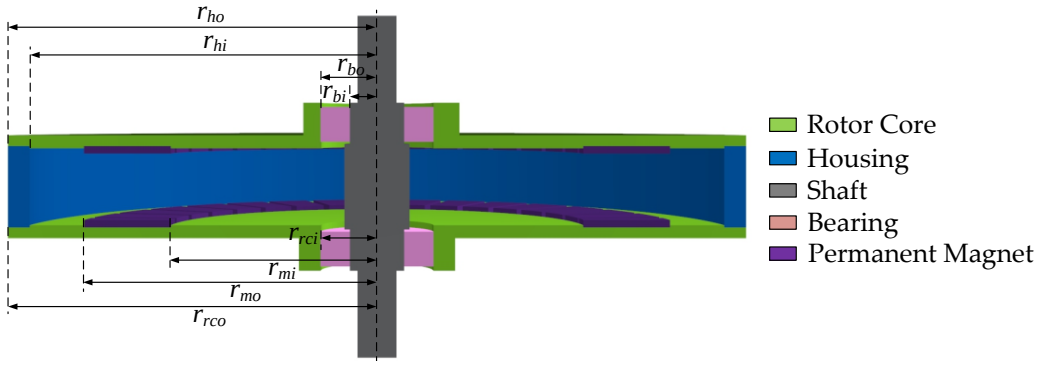

Figure 12. Cross-section of the YASA machine.

3.2.2. Bearing

The bearing connects the stationary part and the rotating part. Figure 13 shows the thermal model of the bearing. P_b represents the friction loss of the bearing. A part of the heat transfers from the bearing to the rotor core and is dissipated. R_{shb} is the thermal resistance between the bearing and shaft, as shown in Figure 9. R_{brc} is the thermal resistance between the bearing and rotor core, as shown in Figure 13. The equations follow:

$$R_{shb} = \frac{(r_{bo} - r_{bi})/2}{\frac{\left(\frac{r_{bo}+r_{bi}}{2} + r_{bi}\right)}{2} 2\pi H_{be} k_{be}} = \frac{(r_{bo} - r_{bi})/2}{\left(\frac{r_{bo}+r_{bi}}{2} + r_{bi}\right)\pi H_{be} k_{be}} \tag{24}$$

$$R_{brc} = \frac{(r_{bo} - r_{bi})/2}{\left(\frac{r_{bo}+r_{bi}}{2} + r_{bo}\right)\pi H_{be} k_{be}} \tag{25}$$

where r_{bo} and r_{bi} are the outer and inner radius of the bearing, respectively, and k_{be} is the equivalent thermal conductivity of the bearing.

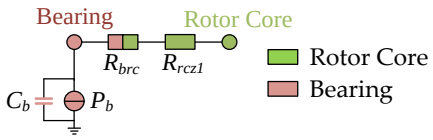

Figure 13. Bearing thermal model.

R_{rcz1} is the thermal resistance of the rotor core. Assuming the rotor core and the permanent magnet are the same distance to the shaft, then:

$$R_{rcz1} = \frac{r_{rcma} - r_{rci}}{(r_{rcma} + r_{rci})\pi H_{rc} k_{rc}} \tag{26}$$

where r_{rcma} is the distance from the permanent magnet to the shaft center, R_{rci} is the inner radius of the rotor core, which is equal to the outer radius of the bearing, H_{rc} is the height of the rotor core, and k_{rc} is the thermal conductivity of the rotor core.

3.2.3. Rotor Core

The eddy current loss of the rotor core is calculated by the FE method. Figure 14 shows the thermal model of the rotor core, which contacts the inner-air and surroundings directly. R_{rcia} is the convective thermal resistance between the rotor core and inner-air, R_{rcso} is the convective thermal resistance between the rotor core and surroundings, R_{rcz2} is the thermal resistance of the rotor core, and R_{hy} is the axial thermal resistance of the housing. The calculation formulae follow:

$$R_{rcia} = \frac{1}{k_{rcia} S_{rcia}} \tag{27}$$

$$S_{rcia} = \pi\left(r_{hi}^2 - r_{mo}^2\right) + \pi\left(r_{mi}^2 - r_{rci}^2\right) \tag{28}$$

$$R_{rcso} = \frac{1}{k_{rcso} S_{rcso}} \tag{29}$$

$$S_{rcso} = \pi\left(r_{rco}^2 - r_{rci}^2\right) \tag{30}$$

$$R_{rcz2} = \frac{r_{rco} - r_{rcma}}{(r_{rcma} + r_{rco})\pi H_{rc} k_{rc}} \tag{31}$$

$$R_{hy} = \frac{H_h/4}{\pi(r_{ho}^2 - r_{hi}^2)k_h} \tag{32}$$

where k_{rci} is the convective heat transfer c between the rotor core and inner-air, and k_{rcso} is the convective efficient heat transfer coefficient between the rotor core and surroundings. S_{rcia} is the contact area between the rotor core and inner-air, S_{rcso} is the contact area between the rotor core and surroundings; r_{mo} and r_{mi} are the outer and inner radius of the permanent magnet, respectively; r_{ho} and r_{hi} are the outer and inner radius of the housing, respectively; H_h is the height of the housing; and k_h is the thermal conductivity of the housing.

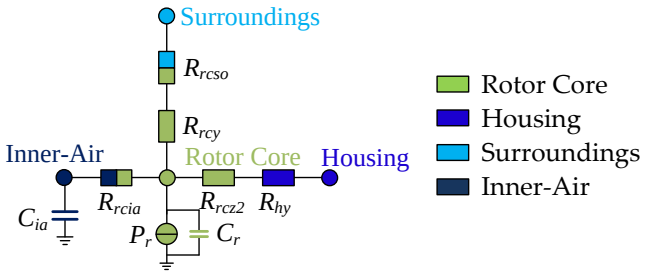

Figure 14. Thermal model of the rotor core.

3.2.4. Housing

There is heat convection between the inner surface of the housing and inner-air. The outer surface contacts with the surroundings, which dissipate heat directly. Figure 15 shows the thermal model of the housing. R_{hz} is the radial thermal resistance of housing, R_{hia} is the convective thermal resistance between the housing and inner-air, and R_{hso} is the convective thermal resistance between the housing and surroundings. The formulas follow:

$$R_{hia} = \frac{1}{S_{hia} k_{hia}} \tag{33}$$

$$S_{hia} = \pi r_{hi} H_h \tag{34}$$

$$R_{hso} = \frac{1}{S_{hso} k_{hso}} \tag{35}$$

$$S_{hso} = \pi r_{ho} H_h \tag{36}$$

$$R_{hz} = \frac{(r_{ho} - r_{hi})/2}{\left(\frac{r_{ho}+r_{hi}}{2}\right)2\pi\frac{H_h}{2}k_h} = \frac{r_{ho} - r_{hi}}{(r_{ho} + r_{hi})\pi H_h k_h} \tag{37}$$

where k_{hia} is the convective heat transfer coefficient between the housing and inner-air, k_{hso} is the convective heat transfer coefficient between the housing and surroundings, S_{hia} is the contact area between the housing and inner-air, and S_{hso} is the contact area between the housing and surroundings.

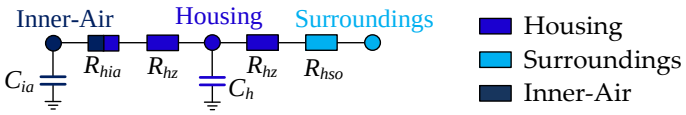

Figure 15. Housing thermal model.

3.3. Entire Thermal Model of the YASA Machine

Based on the thermal models of all the components described above, the entire thermal model of the YASA machine can be obtained by simply integrating all of them, as shown in Figure 16. The thermal model of each component marked with different colors is connected by thermal resistances (including conduction thermal resistance and convective thermal resistance). Between the shaft and the supporting frame, there is the conduction thermal resistance R_{sush}. The thermal model of the bearing and shaft is connected by the thermal resistance R_{shb}. The permanent magnet adheres to the rotor core, so there is the conduction thermal resistance R_{mrc}. Additionally, there are the convective thermal resistances (including R_{mia}, R_{scia}/Q, and R_{wia}/Q) of the YASA machine between the permanent magnet, stator core, armature winding, and inner-air. These thermal resistances are calculated by the formulae given above.

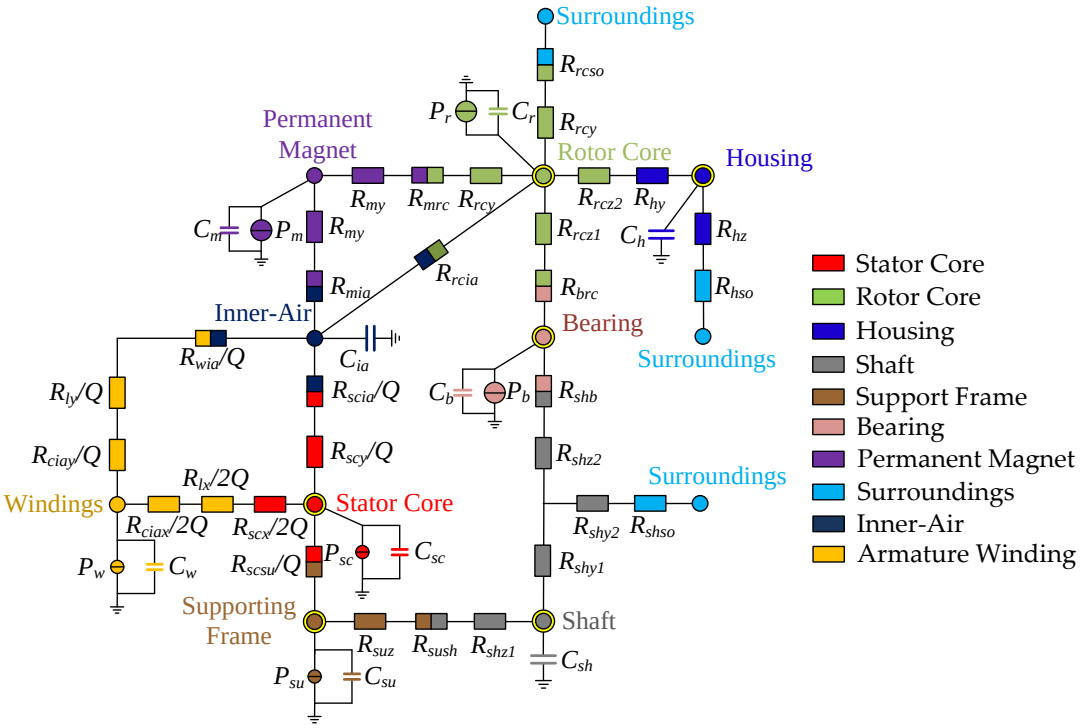

Figure 16. Entire thermal model of the YASA machine.

4. Parameter Calculation of the Thermal Network Model

In this section, the losses of the YASA machine (including the armature winding loss, stator core loss, rotor core loss, permanent magnet eddy current loss, and mechanical loss), the thermal resistance of the air gap, and convective heat transfer coefficient on the hub

surface are calculated. Finally, the detailed temperature distribution of the YASA machine is obtained.

4.1. Losses Calculation

The copper loss is calculated by

$$P_{copper} = mI_s^2 R_s \tag{38}$$

where m is the phase number, R_s is the phase resistance, and I_s is the effective value of phase current.

The core loss separation model proposed by Italian scholar Bertotti [26] is widely used. It mainly includes hysteresis loss, classical eddy current loss, and excess loss:

$$P_{Fe} = P_h + P_c + P_e = K_h f B_m^{\propto} + \frac{\sigma d^2}{12\rho}\frac{1}{T}\int_0^T \left(\frac{dB(t)}{dt}\right)^2 dt + \frac{\sqrt{\sigma G V_0 S}}{\rho}\frac{1}{T}\int_0^T \left(\frac{dB(t)}{dt}\right)^{1.5} dt \tag{39}$$

The core loss is related to magnetic flux density. When the magnetic flux density changes sinusoidally and remagnetization is adopted, Equation (39) can be simplified as

$$P_{Fe} = K_h f B_m^{\propto} + K_c f^2 B_m^2 + K_e f^{1.5} B_m^{1.5} \tag{40}$$

where K_h, K_c, and K_e are the coefficient of hysteresis loss, eddy current loss, and excess loss, respectively; f is the electrical frequency and B_m is the amplitude of magnetic flux density.

Eddy current loss of the rotor core and permanent magnet can be calculated by

$$P_{eddy} = \frac{1}{\sigma}\int J^2 dV \tag{41}$$

where σ is the conductivity, J is the eddy current density, and V is the volume of the component.

Mechanical loss includes bearing loss P_b and wind friction loss P_{wind}. The formula follows:

$$P_b = 0.06 k_{fb}(m_r + m_{sh}) n_s \tag{42}$$

where k_{fb} is an empirical coefficient, which in the range 1–3 m^2/s^2; m_r, m_{sh} is the mass of rotor and shaft, respectively; n_s is the rotating speed.

$$P_{wind} = \frac{1}{2} c_f \rho_{cm} (2\pi n_s)^3 \left(R_{out}^5 - R_{sh}^5\right) \tag{43}$$

where ω_s is electric angular speed; V_{air} is the dynamic viscosity of air, taken as 2×10^{-5} Pas; and ρ_{cm} is the air density, taken as 1.2 kg/m^3. R_{out} is the outer radius of the rotor and R_{sh} is the outer radius of the shaft.

4.2. Air Gap Thermal Resistance and Convective Heat Transfer Coefficient on the Hub Surface

The calculation process of the air gap thermal resistance follows four points:

(1) Reynolds number R_{eg} of the air gap is determined according to machine radius, speed, and dynamic viscosity of the fluid, as shown in Equation (44) [27].

(2) The fluid types are determined by Reynolds number R_{eg}, which generally includes laminar flow, transition flow, and turbulent flow [28].

(3) Determination of the Nusselt constant N_u is based on Reynolds number R_{eg} and the air gap ratio G ($G = g/R_2$, where g is the distance between the stator and rotor plate, R_2 is the outer radius of the rotating plate), as shown in Table 2 [29].

Table 2. Nusselt constant function relationship.

Value Range	Fluid Type	Formula
G = 0.01	Laminar flow	$Nu = 7.46Re_g^{0.32}$
$0.02 \leq G \leq 0.06$	Laminar flow	$Nu = 0.50\left(1 + 5.47 \times 10^{-4} exp(112G)\right)Re_g^{0.5}$
$G \geq 0.06$	Laminar flow	$Nu = 0.55\left(1 + 0.462exp\left(\frac{-13G}{3}\right)\right)Re_g^{0.5}$
Rotor plate	Laminar flow	$Nu = 0.55Re_g^{0.5}$
G = 0.01	Turbulence	$Nu = 0.044Re_g^{0.75}$
$0.02 \leq G \leq 0.06$	Turbulence	$Nu = 0.033(12.57exp(-33.18G))Re_g^{3/5+25G^{12/7}}$
$G \geq 0.06$	Turbulence	$Nu = 0.0208(1 + 0.298exp(-9.27G))Re_g^{0.8}$
Rotor plate	Turbulence	$Nu = 0.0208Re_g^{0.8}$

(4) According to this derivation, the air-gap equivalent convective heat transfer coefficient h_g and the air-gap thermal resistance R_g can be obtained by Formulae (46) and (47).

$$Re_g = \frac{\omega_s R_{out}^2}{v_{air}} \tag{44}$$

$$c_f = \frac{3.87}{\sqrt{Re_g}} \tag{45}$$

$$h_g = \frac{Nu \times k_{air}}{R_2} \tag{46}$$

$$R_g = \frac{1}{\pi\left(R_2^2 - R_1^2\right)h_g} \tag{47}$$

where k_{air} is the thermal conductivity of air and R_1 is the inner radius of the rotating plate.

There is no barrier between the end cap and the surroundings, which belongs to heat convection. The convective heat transfer coefficient on the surface of the rotor plate can be obtained by Equation (46).

The average Nusselt constant is obtained from two cases. One is that the airflow type on the surface of the rotor plate is laminar flow, so the average Nusselt constant N_{u1} is calculated by

$$Nu_1 = \frac{2}{5}\left(Re_g^2 + Gr\right)^{\frac{1}{4}} \tag{48}$$

$$Gr = \frac{\beta g R^3 \pi^{3/2} \Delta T}{v^2} \tag{49}$$

where β is the coefficient of thermal expansion; v is the kinematic viscosity coefficient of the fluid, taken as 1.569×10^{-5} m^2/s. ΔT is the temperature difference between the rotor plate surface and the surroundings.

The other airflow type is a combination of laminar flow and turbulence:

$$Nu_1 = 0.15Re_g^{\frac{4}{5}} - 100\left(\frac{r_c}{R_2}\right)^2 \tag{50}$$

$$r_c = \sqrt{2.5 \times 10^5 v/\omega_s} \tag{51}$$

where r_c is the transition radius.

In addition, with the help of the naphthalene sublimation experiment and analogy theory, the relation between the convective heat transfer coefficient and the speed of the rotor plate is obtained by fitting. This paper refers to this method to obtain the convective heat transfer coefficient of the end cap:

$$h_g = 8.859\omega_s^{0.5} \tag{52}$$

The convective heat transfer between the housing and surroundings is calculated by

$$h_p = \frac{k_{air}}{D_2} Nu_2 \tag{53}$$

$$Nu_2 = 0.133 Re_D^{2/3} Pr^{1/3} \tag{54}$$

$$Re_D = \frac{\omega_s D_2^2}{v} \tag{55}$$

where h_p, $N_{u2,}$ and Re_D are the convective heat transfer coefficient, average Nusselt constant, and Reynolds number of the rotor plate, respectively. D_2 is the outer diameter of the rotor plate; P_r is the Prandtl number of the air, taken as 0.703.

The inner-air thermal resistance, the convective heat transfer coefficient between the rotor core and surroundings, and the convective heat transfer coefficient between the housing and surroundings are 0.7568 K/w, 62.8 w/(m^2·K), and 47.8 w/(m^2·K), respectively.

4.3. Results of the Thermal Network Model

The temperature distribution of the YASA machine can be obtained by the entire thermal network model. The temperature of all the components is listed in Table 3.

Table 3. The steady-state temperature of the YASA machine.

Machine Components	Steady-State Temperature (°C)
Winding	127.07
Stator core	100.57
Permanent magnet	54.54
Rotor core	52.00
Housing	49.35
Bearing	63.61

It can be found that the armature winding temperature is the highest and the temperature of the stator core is lower than that of the winding temperature. The lowest temperature is the housing and rotor core. The armature winding is the main heat source of the YASA machine. The stator core and winding are located in the center of the machine, from which dissipation of heat is difficult. The rotor core and the housing are contacted directly by the surroundings, which makes its lower temperature rise. Under the rated condition, the temperature of the permanent magnet is 54.54 °C. The temperature does not exceed the allowable working temperature, which ensures reliable operation.

By setting the laboratory temperature at 20 °C, all components of the YASA machine tend to be stable at 80 min, as shown in Figure 17.

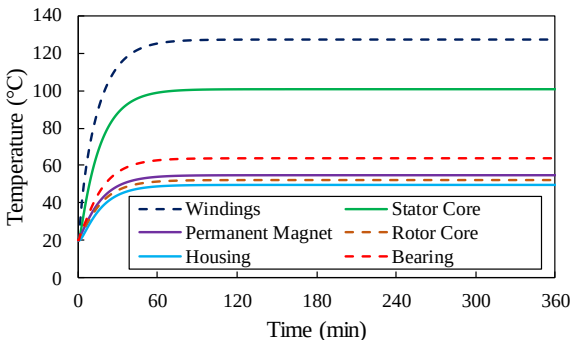

Figure 17. The transient temperature rise of the YASA machine.

5. Experimental Verification

5.1. Experimental Prototype

The prototype is shown in Figure 18. The segmented stator core and armature winding are fixed by the support frame, as shown in Figure 18a. Permanent magnets are bonded to the rotor core, as shown in Figure 18b. The YASA machine assembled is shown in Figure 18c.

(**a**) (**b**) (**c**)

Figure 18. YASA machine assembly: (**a**) stator; (**b**) rotor; (**c**) machine assembly.

5.2. Prototype Experiment

The rated 11 A direct current (DC) corresponding 5 A/mm^2 current density is applied to the armature winding. The experimental data of the YASA machine are compared with the calculated results of the LPTN model, and the results are in good agreement, as shown in Figure 19.

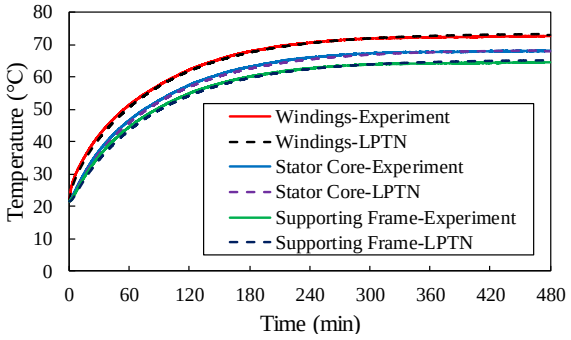

Figure 19. Instantaneous temperature-rise test of the prototype under 11 A DC.

Further, the direct current with different values is applied to the windings to measure the temperature rise of the YASA machine. The current is disconnected after a period of time, the cooling curve is measured, and the results are compared with the thermal network, as shown in Figures 20–22. The maximum error is less than 2.5 °C, which occurs in the armature windings. The error mainly comes from the change in environmental temperature and the given error of heat capacity. The error is smaller than that of the LPTN model for the single-sided AFPM machine proposed in [17], whose temperature error is 4 °C.

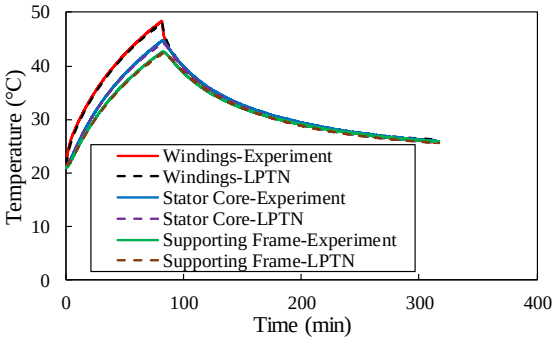

Figure 20. Instantaneous temperature-rise test of the prototype under 10 A DC.

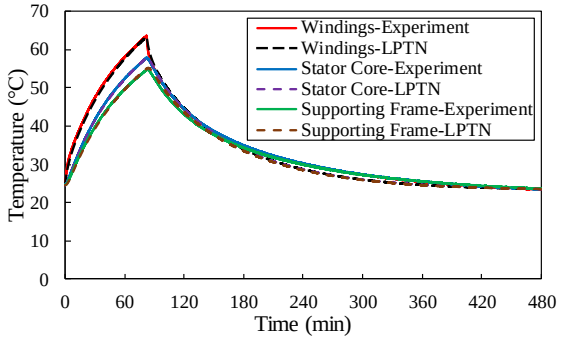

Figure 21. Instantaneous temperature-rise test of the prototype under 12 A DC.

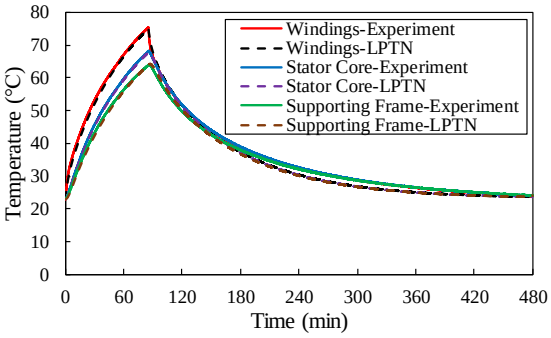

Figure 22. Instantaneous temperature-rise test of the prototype under 13.5 A DC.

6. Summary

In this paper, the LPTN model of the YASA machine for in-wheel traction application is developed to calculate the temperature distribution of all components of the YASA machine. The thermal models of all components in YASA machines, including the stationary and rotary components, are simplified based on the symmetrical structure, while the detailed thermal resistance formulae are given. Based on the loss results calculated by electromagnetic FE analysis, the temperature distribution of the YASA machine is obtained. Comparing the calculated and experimental results, the maximum temperature difference is no more than 3.3%, which validates very good accuracy of the proposed thermal model. The proposed method is considered as a good reference for design engineers of YASA machines in the applications of in-wheel traction. In addition, this paper is also beneficial to the research of machine cooling. The advanced cooling technique of the YASA machine applied on in-wheel traction systems will be investigated in a following study.

Author Contributions: Conceptualization, H.Z.; methodology, G.W.; validation, Y.W. and G.W.; investigation, G.W., Y.W. and Q.N.; data curation, Y.W.; writing—original draft preparation, G.W.; writing—review and editing, Y.G. and Q.N.; visualization, W.H.; supervision, W.H. and H.Z.; project administration, W.H. All authors have read and agreed to the published version of the manuscript.

Funding: This research was funded by The National Key Research and Development Program of China grant number 2021YFB2500703.

Institutional Review Board Statement: Not applicable.

Informed Consent Statement: Not applicable.

Data Availability Statement: Not applicable.

Conflicts of Interest: The authors declare no conflict of interest.

References

1. Chang, J.; Fan, Y.; Wu, J. A Yokeless and Segmented Armature Axial Flux Machine with Novel Cooling System for In-Wheel Traction Applications. *IEEE Trans. Ind. Electron.* **2021**, *68*, 4131–4140. [CrossRef]
2. Taran, N.; Klink, D.; Heins, G. A Comparative Study of Yokeless and Segmented Armature Versus Single Side Axial Flux PM Machine Topologies for Electric Traction. *IEEE Trans. Ind. Appl.* **2022**, *58*, 325–335. [CrossRef]
3. Li, T.; Liang, X.; Dou, H. Thermal Analysis of the Yokeless and Segmented Armature Axial Flux In-wheel motor. In Proceedings of the 2020 International Conference on Artificial Intelligence and Computer Engineering (ICAICE), Beijing, China, 23–25 October 2020; pp. 449–452.
4. Zhang, B.; Seidler, T.; Dierken, R.; Doppelbauer, M. Development of a Yokeless and Segmented Armature Axial Flux Machine. *IEEE Trans. Ind. Electron.* **2016**, *63*, 2062–2071. [CrossRef]
5. Xu, L.; Xu, Y.; Gong, J. Analysis and Optimization of Cogging Torque in Yokeless and Segmented Armature Axial-Flux Permanent-Magnet Machine with Soft Magnetic Composite Core. *IEEE Trans. Magn.* **2018**, *54*, 8106005. [CrossRef]
6. Geng, W.; Zhang, Z.; Li, Q. High Torque Density Fractional-Slot Concentrated-Winding Axial-Flux Permanent-Magnet Machine with Modular SMC Stator. *IEEE Trans. Ind. Appl.* **2019**, *56*, 3691–3699.
7. Geng, W.; Wang, Y.; Wang, J. Comparative Study of Yokeless Stator Axial-Flux PM Machines having Fractional Slot Concentrated and Integral Slot Distributed Windings for Electric Vehicle Traction Applications. *IEEE Trans. Ind. Electron.* 2022; *early access*.
8. Wang, Y.; Lu, J.; Liu, C.; Lei, G.; Guo, Y.; Zhu, J. Development of a High-Performance Axial Flux PM Machine with SMC Cores for Electric Vehicle Application. *IEEE Trans. Magn.* **2019**, *55*, 8105304. [CrossRef]
9. Kim, J.; Lee, J.; Song, J. Characteristics Analysis Method of Axial Flux Permanent Magnet Motor Based on 2-D Finite Element Analysis. *IEEE Trans. Magn.* **2017**, *53*, 8105304. [CrossRef]
10. Gerlando, A.; Foglia, G.; Iacchetti, M.; Perini, R. Parasitic Currents in Stray Paths of Some Topologies of YASA AFPM Machines: Trend with machine size. *IEEE Trans. Ind. Electron.* **2016**, *63*, 2746–2756. [CrossRef]
11. Camilleri, R.; Howey, D.A.; McCulloch, M.D. Predicting the Temperature and Flow Distribution in a Direct Oil-Cooled Electrical Machine with Segmented Stator. *IEEE Trans. Ind. Electron.* **2016**, *63*, 82–91. [CrossRef]
12. Vansompel, H.; Leijnen, P.; Sergeant, P. Multiphysics Analysis of a Stator Construction Method in Yokeless and Segmented Armature Axial Flux PM Machines. *IEEE Trans. Energy Convers.* **2019**, *34*, 139–146. [CrossRef]
13. Fawzal, A.S.; Cirstea, R.M.; Gyftakis, K.N. Fan Performance Analysis for Rotor Cooling of Axial Flux Permanent Magnet Machine. *IEEE Trans. Ind. Appl.* **2017**, *53*, 3295–3304. [CrossRef]
14. Luo, L.; Chang, J.; Wu, J. Design and Analysis of a Water-Cooling System in a New Yokeless and Segmented Armature Axial In-Wheel Motor for Electric Vehicles. *J. Therm. Sci. Eng. Appl.* **2021**, *13*, 1–12. [CrossRef]
15. Le, W.; Lin, M.; Lin, K. A Novel Stator Cooling Structure for Yokeless and Segmented Armature Axial Flux Machine with Heat Pipe. *Energies* **2021**, *14*, 5717. [CrossRef]
16. Le, W.; Lin, M.; Jia, L. Design of a Novel Stator Water-Cooling System for Yokeless and Segmented Armature Axial Flux Machine. In Proceedings of the 2021 IEEE 4th Student Conference on Electric Machines and Systems (SCEMS), Huzhou, China, 2–3 December 2021; pp. 1–4.
17. Winterborne, D.; Stannard, N.; Sjöberg, L. An Air-Cooled YASA Motor for in-Wheel Electric Vehicle Applications. *IEEE Trans. Ind. Appl.* **2020**, *56*, 6448–6455. [CrossRef]
18. Vansompel, H.; Hemeida, A.; Sergeant, P. Stator Heat Extraction System for Axial Flux Yokeless and Segmented Armature Machines. In Proceedings of the 2017 IEEE International Electric Machines and Drives Conference (IEMDC), Miami, FL, USA, 21–24 May 2017; pp. 1–7.
19. Burke, R.; Giedymin, A.; Wu, Z. A Lumped Parameter Thermal Model for Single-Sided AFPM Machines with Experimental Validation. *IEEE Trans. Ind. Electron.* **2020**, *6*, 1065–1083. [CrossRef]
20. Mohamed, A.; Hemeida, A.; Vansompel, H. Parametric Studies for Combined Convective and Conductive Heat Transfer for YASA Axial Flux Permanent Magnet Synchronous Machines. *Energies* **2018**, *11*, 2983. [CrossRef]

21. Mohamed, A.H.R.; Vansompel, H.; Hemeida, A. Transient Lumped Parameter Thermal Model Based Load ability Studies for The YASA Axial Flux Permanent Magnet Synchronous Machines. In Proceedings of the Young Researchers Symposium, Brussels, Belgium, 25–25 May 2018.
22. Chen, Q.; Liang, D.; Gao, L. Hierarchical Thermal Network Analysis of Axial-flux Permanent-Magnet Synchronous Machine for Electric Motorcycle. *IET Electr. Power Appl.* **2018**, *12*, 859–866. [CrossRef]
23. Mohamed, A.H.; Hemeida, A.; Rashekh, A. A 3D Dynamic Lumped Parameter Thermal Network of Air-Cooled YASA Axial Flux Permanent Magnet Synchronous Machine. *Energies* **2018**, *11*, 774. [CrossRef]
24. Zhang, H.; Giangrande, P.; Sala, G. Thermal Model Approach to Multisector Three-Phase Electrical Machines. *IEEE Trans. Ind. Electron.* **2021**, *4*, 2919–2930. [CrossRef]
25. Staton, D.; Boglietti, A.; Cavagnino, A. Solving the More Difficult Aspects of Electric Motor Thermal Analysis in Small and Medium Size Industrial Induction Motors. *IEEE Trans. Energy Convers.* **2005**, *20*, 620–628. [CrossRef]
26. Bertotti, G. General properties of power losses in soft ferromagnetic materials. *IEEE Trans. Magn.* **1988**, *24*, 621–630. [CrossRef]
27. Howey, D.A.; Childs, P.R.N.; Holmes, A.S. Air-gap Convection in Rotating Electrical Machines. *IEEE Trans. Ind. Electron.* **2012**, *59*, 1367–1375. [CrossRef]
28. Owen, J.M.; Haynes, C.M.; Bayley, F.J. Heat Transfer from an Air-Cooled Rotating Disk. *Proc. R. Soc. Lond. A Math. Phys. Sci.* **1974**, *336*, 453–473.
29. Boutarfa, R.; Harmand, S. Local Convective Heat Transfer for Laminar and Turbulent Flow in a Rotor-Stator System. *Exp. Fluids* **2005**, *38*, 209–221. [CrossRef]